Sensors & Actuators: B. Chemical 350 (2022) 130882

Contents lists available at ScienceDirect

Sensors and Actuators: B. Chemical

journal homepage: www.elsevier.com/locate/snb

# A FRET pair for quantitative and superresolution imaging of amyloid fibril formation

Álvaro Ruiz-Arias [a], Rocío Jurado [b], Francisco Fueyo-González [c,1], Rosario Herranz [c], Natividad Gálvez [b], Juan A. González-Vera [a,c,*], Angel Orte [a,*]

[a] Departamento de Fisicoquímica, Unidad de Excelencia de Química Aplicada a Biomedicina y Medioambiente, Facultad de Farmacia, Universidad de Granada, Campus Cartuja, 18071, Granada, Spain
[b] Departamento de Química Inorgánica, Universidad de Granada, 18071 Granada, Spain
[c] Instituto de Química Médica (CSIC), Juan de la Cierva 3, 28006 Madrid, Spain

ARTICLE INFO

*Keywords:*
Amyloid fibrils
Protein aggregation
Solvatochromic dyes
Biomarkers
FLIM
STED microscopy

ABSTRACT

The presence of neuritic plaques and amyloid fibrils arising from the misfolding of certain proteins is the principal molecular indicator of neurodegenerative diseases such as Alzheimer's and Parkinson's disease. Methodologies for studying the early stages of amyloid aggregation are rapidly arising to provide a better understanding of the mechanism of fibrillization and cytotoxicity and to identify potential targets for diagnosis and therapy. The method presented here involves the simultaneous use of two different fluorophores, a quinolimide derivative and Nile Blue A. These are capable of interacting with and reporting on the formation of preamyloid aggregates and fibrils of apoferritin through fluorescence resonance energy transfer (FRET), which occurs between them, thus maximizing the contrast in detection and quantitative information of such amyloid species by using multidimensional fluorescence lifetime imaging microscopy (FLIM).

## 1. Introduction

The main molecular hallmark of neurodegenerative diseases such as Alzheimer's and Parkinson's disease is the presence of proteinacous fibrillar plaques in the brain. These plaques are composed of intertwined branches of the so-called amyloid fibrils, which result from aberrant aggregation of certain proteins [1–3]. Amyloid fibrils are usually formed by single or multiple protofilaments, rich in cross-β structure, of several μm in length. The amyloid aggregation process responds to a specific polymerization mechanism, in which early aggregates are well-accepted to be the species responsible for cellular toxicity and inflammation in disease-related protein aggregation [4,5]. For instance, early-stage aggregates of the 42 amino acid β-amyloid peptide (Aβ42), a peptide linked to Alzheimer's disease, are capable of binding cellular membranes and inducing apoptosis [6]. In fact, a critical step in the amyloid fibrillization process and the link with cytotoxic effects is the conformational change that convert the very early soluble aggregates to prefibrillar aggregates and later to mature protofibrils, which are capable of subsequent organized growth [5,7]. Therefore, the development of robust methods for identifying the different stages of protein aggregation is of crucial importance to better understand its mechanism and, importantly, recognize potential therapeutic targets, constituting a very active field of research nowadays [4,8–10].

Although techniques such as electron paramagnetic resonance [9] and atomic force microscopy [10] are arising as alternatives for detecting soluble oligomeric aggregates, the use of fluorescent probes in fluorescence spectroscopy and microscopy techniques is still the methodology most widely used to detect and monitor processes of biological importance, such as aggregation of misfolded proteins, due to its high specificity and sensitivity [11,12]. Amyloid fibril formation has traditionally been studied using thioflavin T (ThT) and Congo Red dyes because they specifically bind to protofibrils and mature fibrils resulting in enhanced light absorption and emission [13]. Nevertheless, early aggregates cannot be specifically detected with these fluorophores because their binding to such species is not strong enough. For this reason, recent studies have provided a wide range of fluorescent dyes

* Corresponding authors at: Departamento de Fisicoquímica, Unidad de Excelencia de Química Aplicada a Biomedicina y Medioambiente, Facultad de Farmacia, Universidad de Granada, Campus Cartuja, 18071, Granada, Spain
*E-mail addresses:* gonzalezvera@ugr.es (J.A. González-Vera), angelort@ugr.es (A. Orte).
[1] Current address: Department of Medicine, Translational Transplant Research Center, Immunology Institute, Icahn School of Medicine at Mount Sinai, New York, USA.

https://doi.org/10.1016/j.snb.2021.130882
Received 4 August 2021; Received in revised form 13 September 2021; Accepted 4 October 2021
Available online 7 October 2021

shown to be capable of detecting different types of amyloid aggregates. A few examples of recent developments of luminescent dyes to stain amyloid aggregates and fibrils, even in cells and tissues, involve curcumine derivatives [14], BODIPY-based dyes [15], molecular rotors [16], oxazine fluorophores [17], benzimidazole derivatives [18], conjugated polythiophenes [19,20], thiazolium dyes [21,22] and ruthenium complexes [23,24], among many others. Some of these examples have been recently revised in references [8,25].

Even though the aforementioned dyes are sensitive tools with which to stain amyloid aggregates, usually, they merely deliver morphological information and cannot provide quantitative data on the structural features of the aggregates. In this context, the use of environment-sensitive fluorophores is a powerful tool for studying protein-protein interactions and amyloid aggregation, since these fluorophores significantly vary their photophysical properties depending on the immediate environment [26]. For instance, the dye Nile red is characterized by weak fluorescence in aqueous environments. However, when it binds to hydrophobic surfaces of proteins, its fluorescence intensity increases considerably. Due to its solvatochromic properties, this dye has been used to map and quantify the hydrophobicity of aggregates associated with disease and other biological structures by extracting both the position of each fluorophore molecule and the emission spectrum simultaneously [27,28]. In a previous manuscript, we reported a new family of solvatochromic and fluorogenic fluorophores, 9-aminoquinolimides, with the ability to detect different types of preamyloid aggregates, even in zebrafish embryos, using dual-color fluorescence lifetime imaging microscopy (FLIM) [29]. In particular, the dye 9-azetidinyl-quinolimide, **AQui**, showed the best photophysical properties and the best contrast and highest signal-to-noise ratio upon interaction with protein aggregates. Thanks to its spectral shift and enhancement in the fluorescence lifetime, $\tau$, **AQui** demonstrated a high potential for detecting different types of amyloid aggregates. However, the dynamic range of intensity ratio and lifetime values was relatively modest, leaving ample room for improvement. To improve the sensitivity and dynamic range of **AQui** for pre-amyloid aggregate characterization and classification using dual-color FLIM, we envisaged that simultaneous use of two different fluorophores capable of interacting with preamyloid aggregates and reporting on their formation would be a novel and efficient methodology with which to maximize contrast in the detection of such aggregates. Moreover, if fluorescence resonance energy transfer (FRET) is feasible between the pair of dyes, the coexistence of the two dyes in close proximity, within the structure of the amyloid aggregates, would result in a decrease in the $\tau$ for the donor fluorophore (the one emitting at shorter wavelengths) and a red-shift of the overall emission with larger contribution of the acceptor fluorophore (emitting at longer wavelengths). These two effects are easily quantifiable, even for individual aggregates at the single molecule level, using dual-color FLIM [7], and would allow a broader dynamic range and sensitivity for the detection of amyloid aggregates. In fact, the combination of different fluorophores will also allow to establish logical gates for an efficient classification of different amyloidogenic states, as it has been previously described in studies of other physiologically relevant processes [30,31].

To apply these concepts and ideas in the study of amyloid fibrillization, we chose apoferritin as the target protein. The ubiquitous apoferritin, the iron-free ferritin molecule, is a hollow globular protein composed of 24 polypeptide subunits ($M_n \sim 480$ kDa, 12 nm size); its main biological function is to bind and store iron, and it does so by forming iron oxyhydroxide nanoparticles of approximately 6 nm, which are traditionally described as ferrihydrite [32,33]. Apoferritin, a key component of the iron regulatory system in the brain and widely recognized as a crucial protein for iron metabolism, converts into amyloid fibrils with polymorphisms that share common traits with pathological amyloid fibrils found in Alzheimer's and Parkinson's diseases [34,35]. In addition, it has recently been discovered that COVID-19 patients show high levels of the iron-bound protein ferritin in blood, as in other inflammatory states caused by infection [36]. Therefore, herein, we describe new methodologies for studying amyloid aggregation of a physiologically relevant target.

## 2. Experimental section

### 2.1. Preparation of apoferritin samples

The horse spleen apoferritin protein was purchased from Sigma-Aldrich and was used without further manipulation. Protein solutions (0.2 wt%) were adjusted to pH 2 (1 M HCl in Milli-Q water) and then heated (90 °C in hermetically sealed glass tubes). Aliquots of the samples were collected at 1 h, 3 h, 9 h, and 24 h after starting incubation and quenched immediately in an ice–water bath to arrest the conversion of monomers into fibrils. These aliquots were then labeled according to incubation time, stored at 4 °C, and used for structural analysis without further manipulation.

### 2.2. Steady-state fluorimetry

Fluorescence emission spectra were obtained on a Jasco FP-8300 spectrofluorometer (Jasco, Tokyo, Japan), at the excitation wavelengths of $\lambda_{ex} = 470$ nm and $\lambda_{ex} = 485$ nm, for preferential excitation of the **AQui** dye. Fluorophores were added to the aliquots of 30 μM incubating apoferritin samples, at a concentration of 10 μM for **AQui** and 10 μM for Nile blue A (**NBA**), and then the fluorescence spectrum was obtained. Since the dyes were just added before the measurement, photostability of the dyes along the time course of protein incubation and aggregation is not an issue. In any case, both **AQui** and **NBA** showed excellent photostability under continuous irradiation conditions (Figure S1 in the Supplementary Material). Regarding the tests with the FRET pair involving **AQui** and ThT, the same concentrations of protein and dyes were used.

### 2.3. Transmission electron microscopy (TEM)

TEM images were obtained using a Libra 120 Plus TEM microscope (Carl Zeiss SMT, Oberkochen, Germany). Equipped with a LaB6 filament and an SSCCD 2 k × 2 k direct coupling camera, it was operated at 120 kV. TEM images of samples of apoferritin incubated at different times were collected by adding aliquots of protein on Formvar 300-mesh copper grids, washed twice with Milli-Q water and stained with uranyl acetate 1% (w/v).

### 2.4. Multiparametric FLIM

Multiparametric dual-color FLIM was carried out on a MicroTime 200 microscope (PicoQuant GmbH) equipped with two pulsed interleaved excitation lasers at 470 nm and 635 nm. Using a 600DCXR dichroic filter, the fluorescence emission was divided in the green and in the red detection channels, with a 520/35 and a 685/70 bandpass filter, respectively. SymphoTime 32 (PicoQuant GmbH) and FiJi software (distribution of ImageJ [37]) were employed for imaging analysis. Further experimental details can be found in the Supplementary Materials.

### 2.5. Superresolution STED microscopy

A STED-FLIM microscope (Abberior Expert Line, Abberior Instruments GmbH, Germany) has been used for super-resolution imaging experiments with apoferritin fibers. For confocal microscopy measurements we used two pulsed lasers at the wavelengths of excitation of $\lambda_{ex}$= 485 nm (for **AQui**) and $\lambda_{ex}$= 640 nm (for **NBA**), and used two detection bandpass filters; 545/25 for **AQui** and 685/70 for **NBA**. To obtain STED super-resolution images, a pulsed toroidal, 775-nm depletion laser was overlapped within the confocal volume. The size (area) of the raw images obtained were of 9.5 × 9.5 $\mu m^2$, getting a 200 × 200-pixel

resolution. The pixelsize obtained was of 40.0 × 40.0 nm$^2$, using a dwell time (time per pixel) of 30 μs.

## 3. Results and discussion

### 3.1. *AQui and NBA as a suitable FRET pair for amyloid aggregation studies*

To follow the amyloidogenic aggregation of apoferritin, we tested different dyes capable of acting as FRET pairs, e.g., quinolimide **AQui** and other fluorophores known to bind amyloid aggregates such as thioflavin T and **NBA** [8,13]. These two dyes are typically employed for staining amyloid fibrils since their emission features change remarkably upon interaction with β-sheet-rich structures, such as insoluble aggregates, plaques or mature fibrils. We focused on finding a pair of fluorophores that exhibited adequate overlap between the absorption spectrum of the acceptor (more red-shifted dye) and the fluorescence emission spectrum of the donor (more blue-shifted dye). Provided the two dyes interacted with amyloid aggregates in close proximity the results of efficient FRET would be measurable; these are quenching of the donor fluorophore and enhancement of the acceptor emission. Among the different FRET pairs tested (see Supplementary Material, Figure S1), the mixture of **AQui** and **NBA** was the only one exhibiting clear FRET from **AQui** (donor) to **NBA** (acceptor) and notable changes in fluorescence spectral features as aggregation progressed. These two dyes fulfill the spectral overlap conditions to be an efficient FRET pair (Figure S1). The fluorescence emission spectrum seen for the FRET pair when interacting with incubated apoferritin under amyloidogenic conditions (see Supplementary Material) and with excitation at a wavelength giving preferential absorption by **AQui** ($\lambda_{ex}$ = 485 nm) exhibited a clear decrease in the **AQui** signal and a concomitant increase in the **NBA** signal when compared to appropriate controls of incubated apoferritin in the presence of only **AQui** or **NBA** (Figure S1). This suggested that in the presence of apoferritin prefibrillar aggregates or amyloid fibrils, which present crooked surfaces with many hydrophobic grooves, both dyes bind to these structures and simultaneously interact by placing themselves at a distance close enough to produce effective FRET from **AQui** to **NBA** (Fig. 1).

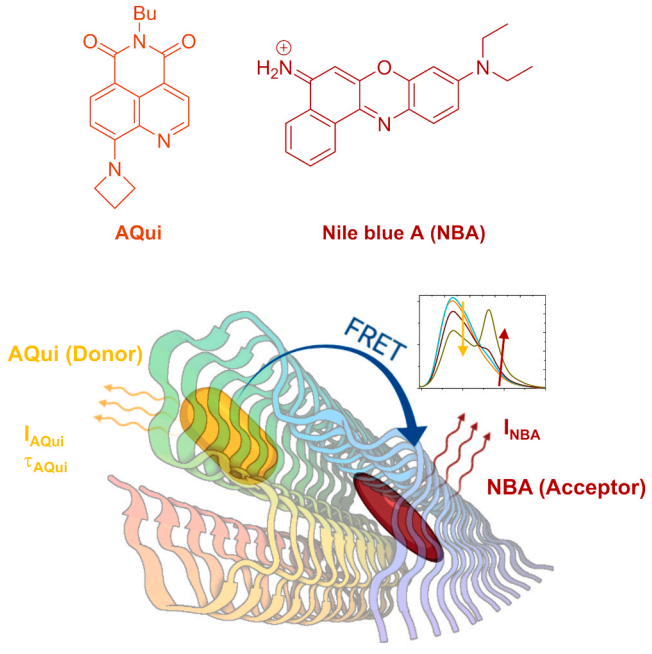


**Fig. 1.** Chemical structures of quinolimide **AQui** and **NBA** and schematic representation of the FRET process that occurs between the dyes on the hydrophobic surfaces of apoferritin fibrils, resulting in quenching of the **AQui** emission (both intensity, $I_{AQui}$, and lifetime, $\tau_{AQui}$) and enhancement of **NBA** emission ($I_{NBA}$).

Next, we studied the apoferritin aggregation process by adding a 1:1 ratio of the FRET pair **AQui**:**NBA** (10 μM) to apoferritin samples (30 μM) previously incubated under amyloidogenic conditions at different times (0, 1, 3, 9, and 24 h). To verify that the aggregation process proceeded until the formation of mature fibrils, TEM images of apoferritin samples incubated at different times were obtained, which showed the formation of long, straight amyloid fibrils after 9 and 24 h of incubation, whereas only short protofibrillar structures were detected in the first hour of incubation (Fig. 2a). The aliquots taken to collect these images contained the fluorophores **AQui** and **NBA**, which were added at the time of pipetting and before mounting on the TEM grid; this is consistent with experiments performed in the absence of the dyes (Figure S2) and in previous reports on amyloid fibrils of apoferritin [35,38]. Importantly, the efficiency of the FRET between the two fluorophores became larger with increasing incubation time, as evidenced by the emission spectra (Fig. 2b). These spectra showed a time-dependent decrease in the **AQui** signal and an increase in the **NBA** emission. The existence of FRET was unequivocally verified by measuring the fluorescence lifetime, τ, of the donor fluorophore, since energy transfer results in faster deactivation dynamics and thus in shortened lifetime values. Fig. 2c shows the decrease in the τ of **AQui** with increasing apoferritin incubation time when the acceptor **NBA** was added. Importantly, these decreases in **AQui** τ values with incubation time, which indicated more efficient FRET, allowed sensitive monitoring of the aggregation process with time-resolved fluorescence techniques. In contrast, in the absence of **NBA**, very small changes were detected in the **AQui** lifetime upon aggregation of apoferritin, as previously found with other proteins [29].

It is important to note that the interaction of **AQui** and **NBA** is not specific for apoferritin aggregates. We previously published that **AQui** can interact with other types of proteins, exhibiting fluorescence enhancement. A similar enhancement occurs for **NBA** when interacting with different types of proteins. Therefore, the combination of the two dyes as a FRET pair can be used as a general approach for the detection of protein hydrophobic patches.

### 3.2. *Multiparametric dual-color FLIM studies of apoferritin aggregates*

Once the spectroscopic measurements confirmed the potential of using both the spectral shifts (Fig. 2b) and donor fluorescence lifetimes (Fig. 2c) of the **AQui**:**NBA** FRET pair to follow the aggregation process, we employed multiparametric dual-color FLIM to explore different types of preamyloid aggregates in the apoferritin fibrillization pathway, thereby maximizing the contrast between the different protein aggregation stages. This technique allowed recomposing multidimensional images that included information not only on the fluorescence intensity and fluorescence lifetime, τ, but also on ratiometric measurements of the fluorescence intensities detected in two different channels.

First, we focused on a ratiometric analysis of the fluorescence intensities of the images obtained in two different detection channels: $I_G$ for the emission of **AQui** (520/35 bandpass filter) and $I_R$ for the emission of **NBA** (685/70 bandpass filter). Hence, the $I_G/I_R$ ratio is a direct representation of the FRET efficiency in the **AQui**:**NBA** pair. Fig. 3 clearly shows the shift in the $I_G/I_R$ ratio towards lower values upon apoferritin incubation and formation of aggregates in the initial 1–3 h exhibited totally different features than those detected after 9 or 24 h of incubation. Additional images can be seen in Figure S3. Frequency histograms quantitatively showed this shift. The central positions of the distributions of $I_G/I_R$ ratio values from aggregates detected after 1, 3, 9, and 24 h of incubation were 12.24 ± 0.22, 4.91 ± 0.02, 1.88 ± 0.02, and 1.00 ± 0.01, respectively, as obtained by fitting the distributions to a log-normal function. This method is, therefore, extremely sensitive compared to previous reports in the literature because $I_G/I_R$ values

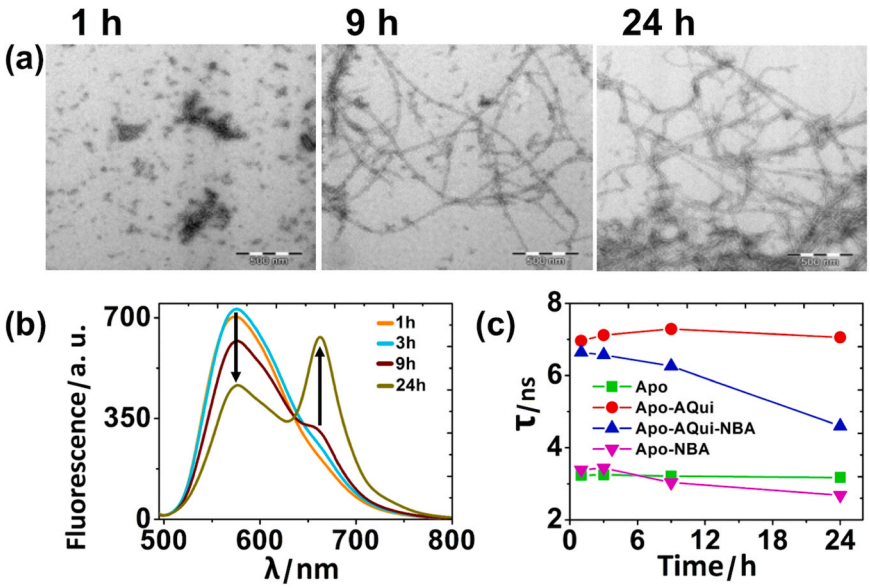


**Fig. 2.** (a) TEM images of apoferritin samples incubated under amyloidogenic conditions at different times (1, 9 and 24 h) to which the FRET pair **AQui**:**NBA** was added. (b) Fluorescence emission spectra of a 1:1 mixture of the FRET pair **AQui**:**NBA** ($\lambda_{ex}$ = 485 nm) added to apoferritin incubated at different times (1, 3, 9 and 24 h). The arrows indicate increasing incubation time. (c) Average fluorescence lifetimes collected at $\lambda_{em}$ = 662 nm, with $\lambda_{ex}$ = 485 nm, of **AQui** (red symbols), **NBA** (magenta symbols), and a 1:1 mixture of the FRET pair **AQui**:**NBA** (blue symbols) in the presence of apoferritin incubated for 1, 3, 9 and 24 h. The values obtained for apoferritin in the absence of any dye is also shown as a control (green symbols).

ranged over one order of magnitude for aggregates of different types [29,39–42].

Following apoferritin amyloid aggregation with fluorescence techniques is particularly challenging because it requires highly acidic pH media (pH < 3); hence, fluorophores that are sufficiently stable and exhibit unchanged emissive properties at highly acidic pH values should be sought. Unfortunately, few commercial dyes emit at low pH values because this is precluded by proton transfer and acid-base reactions. Interestingly, the emission of 9-amino-quinolimide derivatives, such as **AQui**, is not affected by pH in the range 1–13 [29], nor is the emission of **NBA**.

Changes in the fluorescence lifetime of **AQui** due to FRET within amyloid aggregates allowed the use of FLIM to follow the aggregation process. Fig. 4 shows FLIM images of apoferritin aggregates with the **AQui**:**NBA** FRET pair. In particular, we focused on the fluorescence lifetime of the donor in the $I_G$ channel. These images, and those in Figure S4 in the Supplementary Material, clearly exhibited a decrease in $\tau$ as the incubation time of the protein increased, indicating higher FRET

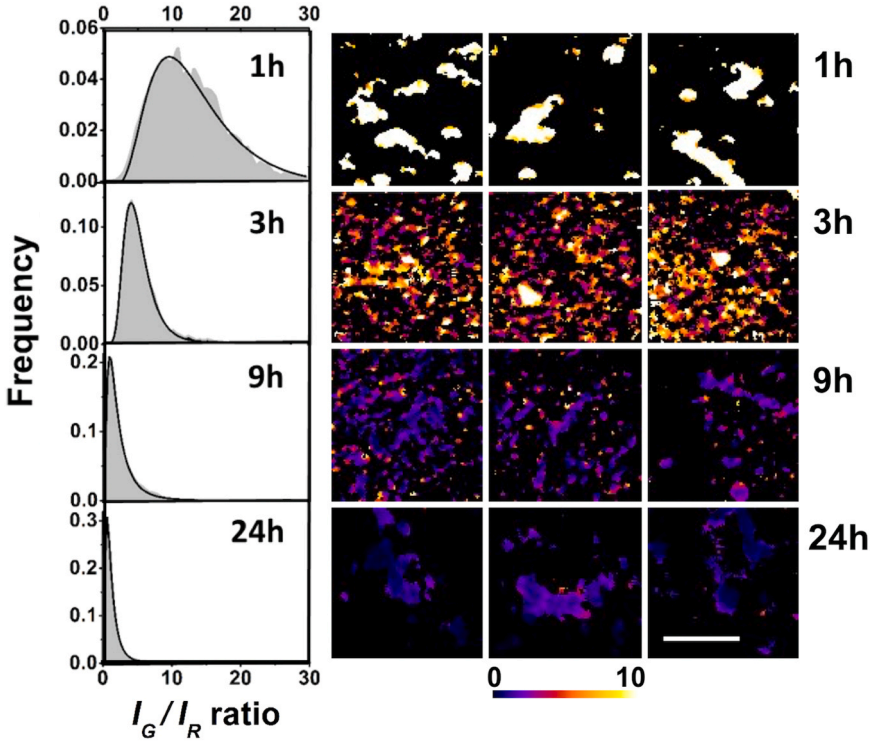


**Fig. 3.** Ratiometric imaging of apoferritin aggregates incubated under amyloidogenic conditions for different times (1, 3, 9 and 24 h), to which **AQui** and **NBA** dyes were added. The scale bar represents 5 μm, and the image sizes are equal in all images. Frequency distributions of the $I_G/I_R$ ratio of detected aggregates, averaged over at least 14 different images, are also shown. The frequency distributions (grey) were fitted to a log-normal function (black curve).

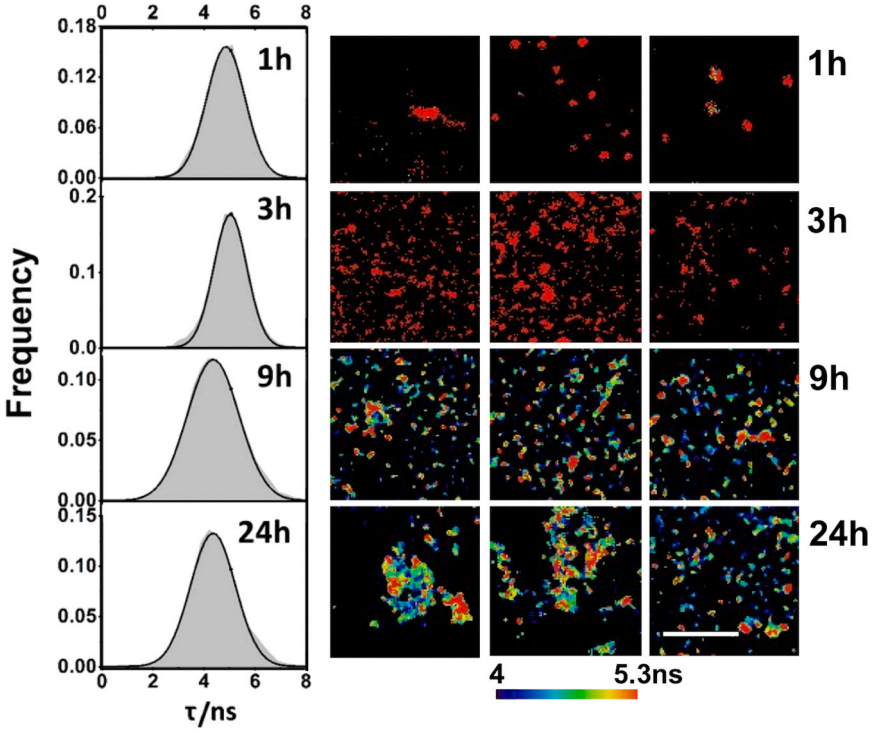


**Fig. 4.** FLIM imaging in the $I_G$ channel of apoferritin aggregates incubated under amyloidogenic conditions for different times (1, 3, 9 and 24 h), to which the **AQui** and **NBA** fluorophores were added. The scale bar represents 5 μm, and image sizes are equal in all images. Frequency distributions of τ for **AQui** in detected aggregates, averaged over at least 14 different images, are also shown. The frequency distributions (grey) were fitted to a Gaussian function (black curve).

efficiency values for aggregates formed in the latest stages. The **AQui** τ distributions (Fig. 4) also displayed differences as a function of incubation time and were centered at 4.85 ± 0.01, 5.02 ± 0.01, 4.35 ± 0.01, and 4.34 ± 0.01 ns for incubation times of 1, 3, 9, and 24 h, respectively. It can be seen that **AQui** τ values were different for different aggregation stages; however, they exhibited less sensitivity than the ratiometric parameter.

The combination of the two fluorophores clearly resulted in improvements in sensitivity for quantitation of different types of aggregates. Whereas **AQui** alone exhibited intensity ratios ranging from 0.7 to 1.6 during the aggregation process, the range was more than one order of magnitude larger for the combination of **AQui** and **NBA**. Likewise, as shown in Fig. 2c, the use of τ to follow the aggregation process exhibited more sensitivity with the FRET pair than with **AQui** only.

Moreover, there were clearly different FRET efficiencies for the two fluorophores within the aggregates with different apoferritin incubation times. This supports the existence of different types of aggregates and protein structures that can be unequivocally revealed using this methodology. Importantly, sharp increases in FRET efficiency were mainly detected at later stages of the aggregation process. This suggests that **NBA** needs specific hydrophobic binding sites that are only formed in advanced stages of aggregation and that the number of hydrophobic pockets on protein surfaces that are exposed during oligomerization increases with incubation time. The late protofibrillar and fibrillar structures entail a more suitable binding environment for **NBA**. In contrast, **AQui** is capable of binding at all stages of aggregation, including soluble oligomeric aggregates, insoluble protofibrillar aggregates, and mature fibrils. As shown in Figures S5 and S6 (see Supplementary Material), the use of the FRET pair **AQui**:**NBA** provided much better sensitivity in both the $I_G/I_R$ ratio and FLIM imaging than did **AQui** alone.

### 3.3. *Super-resolution STED imaging of apoferritin fibrils*

Finally, we used this FRET pair of dyes to image apoferritin amyloid mature fibrils by applying superresolution nanoscopy based on stimulated emission depletion (STED). This technique provides superresolution images through selective deactivation of fluorophores with a high-power, toroidal, near infrared laser pulse, thereby achieving subdiffraction-limited confocal excitation by minimizing the illumination volume [43]. Protein aggregation was recently imaged with STED nanoscopy by imaging amyloid fibrils of α-synuclein with ThT as a fluorescent tag (achieving a spatial resolution ranging 60–70 nm) [44], which showed accumulation of Aβ42 in presynaptic compartments of hippocampal neurons [45]. STED microscopy provides instant superresolution images and does not require image reconstruction, thus eliminating potential artefacts derived from the algorithmic reconstructions required in other superresolution microscopy techniques.

Hence, the binding of **AQui** and **NBA** to preamyloid aggregates and mature fibrils would allow STED imaging throughout the entire aggregation process. Fig. 5 and S7 compare conventional confocal and STED images in the red channel of apoferritin amyloid fibrils incubated under aggregation conditions for 24 h, with the pair of fluorophores, **AQui** and **NBA**, added for imaging. STED images undoubtedly displayed much higher resolutions and the fibrillar structures were distinctly identified, something that is beyond the optical resolution limit of conventional

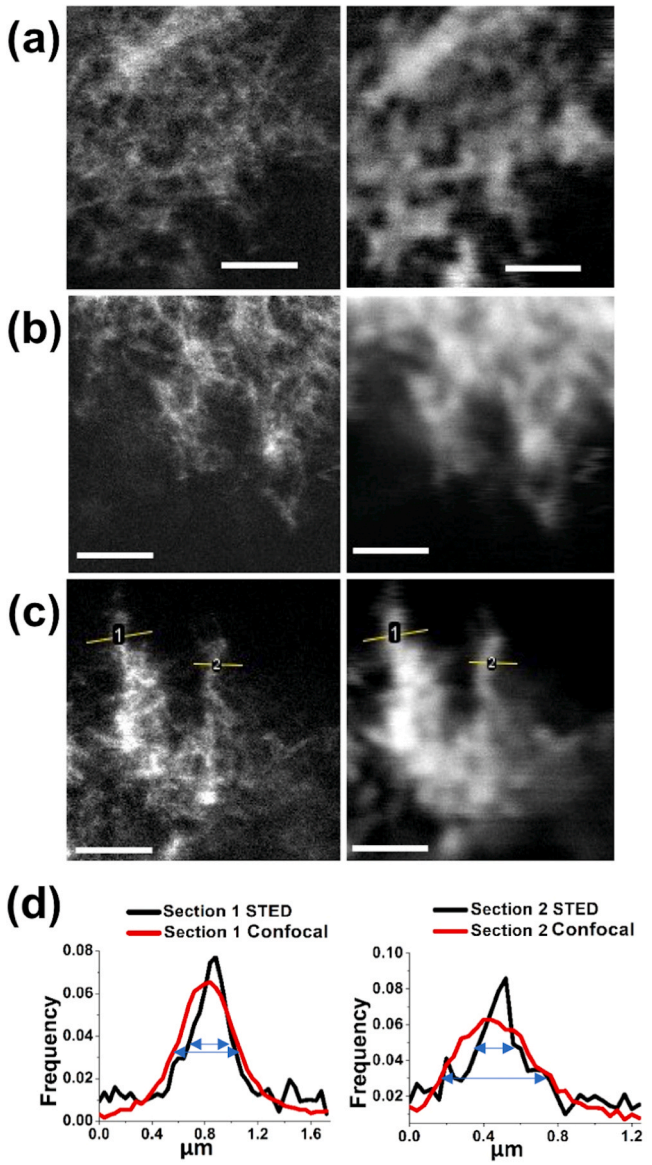


**Fig. 5.** a-c) Different images of mature apoferritin amyloid fibrils with the FRET pair **AQui:NBA**, comparing superresolution STED images (left column) and conventional confocal fluorescence microscopy images (right column). Scale bars represent 2 µm. d) Intensity profiles in the STED images (black lines) and the confocal images (red lines) from readout lines 1 and 2 depicted in panel c).

confocal microscopy. The improvement in resolution is illustrated in Fig. 5d, in which the full width at half maximum (fwhm) values for two sections containing fibrils were compared. Whereas the fwhm values for Sections 1 and 2 were 510 and 575 nm, respectively, in the confocal images, these values decreased to 319 and 260 nm, respectively, in the STED images.

## 4. Conclusions

In this work, we optimized a FRET pair comprising **AQui** as energy donor and **NBA** as energy acceptor for sensitive, quantitative multiparametric dual-color FLIM studies of protein aggregation. Both dyes are capable of binding prefibrillar aggregates of apoferritin, protofibrils and mature amyloid fibrils with different affinities while remaining in close proximity within the aggregates, thus facilitating efficient energy transfer. The fact that **AQui** binds aggregates from the very early stages while **NBA** prefers binding to late protofibrils and fibrils provides enhanced sensitivity for changes in FRET efficiency suitable for quantitative characterization of different types of aggregates.

In conclusion, the methodology proposed here paves the way for the use of many different combinations of fluorophores, which, by precisely modulating their affinities for one or another type of aggregate, can give rise to ultrasensitive detection of critical stages in the misfolded-protein aggregation process with advanced microscopy techniques.

## CRediT authorship contribution statement

Álvaro Ruiz-Arias: Investigation; Formal analysis; Visualization; Writing – original draft. Rocío Jurado: Investigation; Resources; Writing – review & editing. Francisco Fueyo-González: Investigation; Methodology; Resources; Writing – review & editing. Rosario Herranz: Methodology; Resources; Supervision; Writing – review & editing. Prof. Natividad Galvez: Methodology; Resources; Supervision; Funding acquisition; Writing – review & editing. Juan A. González-Vera: Conceptualization; Methodology; Investigation; Formal analysis; Visualization; Supervision; Project administration; Funding acquisition; Writing – original draft. Prof. Angel Orte: Conceptualization; Methodology; Formal analysis; Visualization; Supervision; Project administration; Funding acquisition; Writing – original draft.

## Declaration of Competing Interest

The authors declare that they have no known competing financial interests or personal relationships that could have appeared to influence the work reported in this paper.

## Acknowledgements

This work was supported by grant CTQ2017–85658-R funded by MCIN/AEI/10.13039/501100011033/ FEDER “Una manera de hacer Europa”, and grants PID2019–104366RB-C22 and PID2020–114256RB-I00 funded by MCIN/AEI/10.13039/501100011033. Funding for open access charge: Universidad de Granada / CBUA. We acknowledge the Centro de Instrumentación Científica (CIC) of Universidad de Granada for use of the TEM facilities. Á.R.-A. thanks the Spanish Ministerio de Educación y Formación Profesional for a FPU Ph.D. studentship.

## Appendix A. Supplementary Materials

Supplementary data associated with this article can be found in the online version at doi:10.1016/j.snb.2021.130882.

## References

[1] S.-Y. Ow, D.E. Dunstan, A brief overview of amyloids and Alzheimer’s disease, Protein Sci. 23 (2014) 1315–1331, https://doi.org/10.1002/pro.2524.
[2] D. Eisenberg, M. Jucker, The amyloid state of proteins in human diseases, Cell 148 (2012) 1188–1203, https://doi.org/10.1016/j.cell.2012.02.022.
[3] M.G. Iadanza, M.P. Jackson, E.W. Hewitt, N.A. Ranson, S.E. Radford, A new era for understanding amyloid structures and disease, Nat. Rev. Mol. Cell Biol. 19 (2018) 755–773, https://doi.org/10.1038/s41580-018-0060-8.
[4] S. De, D.C. Wirthensohn, P. Flagmeier, C. Hughes, F.A. Aprile, F.S. Ruggeri, D. R. Whiten, D. Emin, Z. Xia, J.A. Varela, P. Sormanni, F. Kundel, T.P.J. Knowles, C. M. Dobson, C. Bryant, M. Vendruscolo, D. Klenerman, Different soluble aggregates of Aβ42 can give rise to cellular toxicity through different mechanisms, Nat. Commun. 10 (2019) 1541, https://doi.org/10.1038/s41467-019-09477-3.
[5] N. Cremades, S.I.A. Cohen, E. Deas, A.Y. Abramov, A.Y. Chen, A. Orte, M. Sandal, R.W. Clarke, P. Dunne, F.A. Aprile, C.W. Bertoncini, N.W. Wood, T.P.J. Knowles, C. M. Dobson, D. Klenerman, Direct observation of the interconversion of normal and toxic forms of α-synuclein, Cell 149 (2012) 1048–1059, https://doi.org/10.1016/j.cell.2012.03.037.
[6] Á. Ruiz-Arias, J.M. Paredes, C. Di Biase, J.M. Cuerva, M.D. Giron, R. Salto, J. A. González-Vera, A. Orte, Seeding and growth of β-amyloid aggregates upon interaction with neuronal cell membranes, Int. J. Mol. Sci. 21 (2020) 5035, https://doi.org/10.3390/ijms21145035.

[7] F. Castello, J.M. Paredes, M.J. Ruedas-Rama, M. Martin, M. Roldan, S. Casares, A. Orte, Two-step amyloid aggregation: sequential lag phase intermediates, Sci. Rep. 7 (2017) 40065, https://doi.org/10.1038/srep40065.
[8] D. Lee, S.M. Kim, H.Y. Kim, Y. Kim, Fluorescence chemicals to detect insoluble and soluble amyloid-β aggregates, ACS Chem. Neurosci. 10 (2019) 2647–2657, https://doi.org/10.1021/acschemneuro.9b00199.
[9] E. Zurlo, P. Kumar, G. Meisl, A.J. Dear, D. Mondal, M.M.A.E. Claessens, T.P. J. Knowles, M. Huber, In situ kinetic measurements of α-synuclein aggregation reveal large population of short-lived oligomers, PLoS One 16 (2021), e0245548, https://doi.org/10.1371/journal.pone.0245548.
[10] S.E. Sanchez, D.R. Whiten, G. Meisl, F.S. Ruggeri, E. Hidari, D. Klenerman, Alpha synuclein only forms fibrils in vitro when larger than its critical size of 70 monomers, ChemBioChem 22 (2021) 2867–2871, https://doi.org/10.1002/cbic.202100285.
[11] S. Gregoire, J. Irwin, I. Kwon, Techniques for monitoring protein misfolding and aggregation in vitro and in living cells, Korean J. Chem. Eng. 29 (2012) 693–702, https://doi.org/10.1007/s11814-012-0060-x.
[12] H.C. Ishikawa-Ankerhold, R. Ankerhold, G.P.C. Drummen, Advanced fluorescence microscopy techniques - FRAP, FLIP, FLAP, FRET and FLIM, Molecules 17 (2012) 4047–4132, https://doi.org/10.3390/molecules17044047.
[13] C. Xue, T.Y. Lin, D. Chang, Z. Guo, Thioflavin T as an amyloid dye: fibril quantification, optimal concentration and effect on aggregation, R. Soc. Open Sci. 4 (2017), 160696, https://doi.org/10.1098/rsos.160696.
[14] P. Maiti, T.C. Hall, L. Paladugu, N. Kolli, C. Learman, J. Rossignol, G.L. Dunbar, A comparative study of dietary curcumin, nanocurcumin, and other classical amyloid-binding dyes for labeling and imaging of amyloid plaques in brain tissue of 5×-familial Alzheimer's disease mice, Histochem. Cell Biol. 146 (2016) 609–625, https://doi.org/10.1007/s00418-016-1464-1.
[15] L.P. Jameson, S.V. Dzyuba, Aza-BODIPY: improved synthesis and interaction with soluble Aβ1-42 oligomers, Bioorg. Med. Chem. Lett. 23 (2013) 1732–1735, https://doi.org/10.1016/j.bmcl.2013.01.065.
[16] S. Nagarajan, L.J. Lapidus, Fluorescent probe DCVJ shows high sensitivity for characterization of amyloid β-peptide early in the lag phase, ChemBioChem 18 (2017) 2205–2211, https://doi.org/10.1002/cbic.201700387.
[17] M. Hintersteiner, A. Enz, P. Frey, A.-L. Jaton, W. Kinzy, R. Kneuer, U. Neumann, M. Rudin, M. Staufenbiel, M. Stoeckli, K.-H. Wiederhold, H.-U. Gremlich, In vivo detection of amyloid-beta deposits by near-infrared imaging using an oxazine-derivative probe, Nat. Biotechnol. 23 (2005) 577–583, https://doi.org/10.1038/nbt1085.
[18] R. Harada, N. Okamura, S. Furumoto, T. Yoshikawa, H. Arai, K. Yanai, Y. Kudo, Use of a benzimidazole derivative BF-188 in fluorescence multispectral imaging for selective visualization of tau protein fibrils in the Alzheimer's disease brain, Mol. Imaging Biol. 16 (2014) 19–27, https://doi.org/10.1007/s11307-013-0667-2.
[19] T. Klingstedt, K.P.R. Nilsson, Luminescent conjugated poly- and oligo-thiophenes: optical ligands for spectral assignment of a plethora of protein aggregates, Biochem. Soc. Trans. 40 (2012) 704–710, https://doi.org/10.1042/BST20120009.
[20] M. Shahnawaz, A. Mukherjee, S. Pritzkow, N. Mendez, P. Rabadia, X. Liu, B. Hu, A. Schmeichel, W. Singer, G. Wu, A.-L. Tsai, H. Shirani, K.P.R. Nilsson, P.A. Low, C. Soto, Discriminating α-synuclein strains in Parkinson's disease and multiple system atrophy, Nature 578 (2020) 273–277, https://doi.org/10.1038/s41586-020-1984-7.
[21] P. Gaur, M. Galkin, A. Kurochka, S. Ghosh, D.A. Yushchenko, V.V. Shvadchak, Fluorescent probe for selective imaging of α-synuclein fibrils in living cells, ACS Chem. Neurosci. 12 (2021) 1293–1298, https://doi.org/10.1021/acschemneuro.1c00090.
[22] C. Ding, C. Li, Q. Meng, C. Qian, C. Zhang, L. Yang, X. Wang, Y. Wang, A label-free fluorescent probe for dynamic in situ visualization of amyloid-β peptides aggregation, Sens. Actuators B Chem. 347 (2021), 130607, https://doi.org/10.1016/j.snb.2021.130607.
[23] P. Hanczyc, Binuclear ruthenium(II) complexes for amyloid fibrils recognition, Chem. Phys. 445 (2014) 1–4, https://doi.org/10.1016/j.chemphys.2014.10.015.
[24] B. Jiang, A. Aliyan, N.P. Cook, A. Augustine, G. Bhak, R. Maldonado, A.D. Smith McWilliams, E.M. Flores, N. Mendez, M. Shahnawaz, F.J. Godoy, J. Montenegro, I. Moreno-Gonzalez, A.A. Martí, Monitoring the formation of amyloid oligomers using photoluminescence anisotropy, J. Am. Chem. Soc. 141 (2019) 15605–15610, https://doi.org/10.1021/jacs.9b06966.
[25] A. Aliyan, N.P. Cook, A.A. Martí, Interrogating amyloid aggregates using fluorescent probes, Chem. Rev. 119 (2019) 11819–11856, https://doi.org/10.1021/acs.chemrev.9b00404.
[26] A.S. Klymchenko, Solvatochromic and fluorogenic dyes as environment-sensitive probes: design and biological applications, Acc. Chem. Res. 50 (2017) 366–375, https://doi.org/10.1021/acs.accounts.6b00517.
[27] M.N. Bongiovanni, J. Godet, M.H. Horrocks, L. Tosatto, A.R. Carr, D. C. Wirthensohn, R.T. Ranasinghe, J.-E. Lee, A. Ponjavic, J.V. Fritz, C.M. Dobson, D. Klenerman, S.F. Lee, Multi-dimensional super-resolution imaging enables surface hydrophobicity mapping, Nat. Commun. 7 (2016) 13544, https://doi.org/10.1038/ncomms13544.
[28] R. Mishra, D. Sjölander, P. Hammarström, Spectroscopic characterization of diverse amyloid fibrils in vitro by the fluorescent dye Nile red, Mol. Biosyst. 7 (2011) 1232–1240, https://doi.org/10.1039/c0mb00236d.
[29] R. Fueyo-González, F. González-Vera, J.A. Alkorta, I. Infantes, L. Jimeno, M. L. Aranda, P. Acuña-Castroviejo, D. Ruiz-Arias, A. Orte, A. Herranz, Environment-sensitive probes for illuminating amyloid aggregation in vitro and in zebrafish, ACS Sens. 5 (2020) 2792–2799, https://doi.org/10.1021/acssensors.0c00587.
[30] Y. Chen, Y. Wang, Y. Yang, Y. Li, Y. Wang, G. Wang, T.D. James, X. Xuan, H. Zhang, Y. Liu, A molecular-logic gate for COX-2 and NAT based on conformational and structural changes: visualizing the progression of liver disease, Chem. Sci. 11 (2020) 6209–6216, https://doi.org/10.1039/d0sc00574f.
[31] Y. Lv, D. Cheng, D. Su, M. Chen, B.-C. Yin, L. Yuan, X.-B. Zhang, Visualization of oxidative injury in the mouse kidney using selective superoxide anion fluorescent probes, Chem. Sci. 9 (2018) 7606–7613, https://doi.org/10.1039/c8sc03308k.
[32] N.D. Chasteen, P.M. Harrison, Mineralization in ferritin: an efficient means of iron storage, J. Struct. Biol. 126 (1999) 182–194, https://doi.org/10.1006/jsbi.1999.4118.
[33] K. Honarmand Ebrahimi, P.-L. Hagedoorn, W.R. Hagen, Unity in the biochemistry of the iron-storage proteins ferritin and bacterioferritin, Chem. Rev. 115 (2015) 295–326, https://doi.org/10.1021/cr5004908.
[34] R. Jurado, F. Castello, P. Bondia, S. Casado, C. Flors, R. Cuesta, J.M. Domínguez-Vera, A. Orte, N. Gálvez, Apoferritin fibers: a new template for 1D fluorescent hybrid nanostructures, Nanoscale 8 (2016) 9648–9656, https://doi.org/10.1039/c6nr01044j.
[35] R. Jurado, J. Adamcik, M. López-Haro, J.A. González-Vera, Á. Ruiz-Arias, A. Sánchez-Ferrer, R. Cuesta, J.M. Domínguez-Vera, J.J. Calvino, A. Orte, R. Mezzenga, N. Gálvez, Apoferritin protein amyloid fibrils with tunable chirality and polymorphism, J. Am. Chem. Soc. 141 (2019) 1606–1613, https://doi.org/10.1021/jacs.8b11418.
[36] G. Chen, D. Wu, W. Guo, Y. Cao, D. Huang, H. Wang, T. Wang, X. Zhang, H. Chen, H. Yu, X. Zhang, M. Zhang, S. Wu, J. Song, T. Chen, M. Han, S. Li, X. Luo, J. Zhao, Q. Ning, Clinical and immunological features of severe and moderate coronavirus disease 2019, J. Clin. Invest. 130 (2020) 2620–2629, https://doi.org/10.1172/JCI137244.
[37] J. Schindelin, I. Arganda-Carreras, E. Frise, V. Kaynig, M. Longair, T. Pietzsch, S. Preibisch, C. Rueden, S. Saalfeld, B. Schmid, J.-Y. Tinevez, D.J. White, V. Hartenstein, K. Eliceiri, P. Tomancak, A. Cardona, Fiji: an open-source platform for biological-image analysis, Nat. Methods 9 (2012) 676–682, https://doi.org/10.1038/nmeth.2019.
[38] R. Jurado, N. Gálvez, Apoferritin amyloid-fibril directed the in situ assembly and/or synthesis of optical and magnetic nanoparticles, Nanomaterials 11 (2021) 146, https://doi.org/10.3390/nano11010146.
[39] A.K. Mora, S. Murudkar, A. Alamelu, P.K. Singh, S. Chattopadhyay, S. Nath, Benzothiazole-based neutral ratiometric fluorescence sensor for amyloid fibrils, Chem. – A Eur. J. 22 (2016) 16505–16512, https://doi.org/10.1002/chem.201602981.
[40] C. Li, L. Yang, Y. Han, X. Wang, A simple approach to quantitative determination of soluble amyloid-β peptides using a ratiometric fluorescence probe, Biosens. Bioelectron. 142 (2019), 111518, https://doi.org/10.1016/j.bios.2019.111518.
[41] S. Freire, F. Rodríguez-Prieto, M.C. RíosRodríguez, J.C. Penedo, W. Al-Soufi, M. Novo, Towards ratiometric sensing of amyloid fibrils in vitro, Chem. – A Eur. J. 21 (2015) 3425–3434, https://doi.org/10.1002/chem.201406110.
[42] J.-D. Zhang, J. Mei, X.-L. Hu, X.-P. He, H. Tian, Ratiometric detection of β-amyloid and discrimination from lectins by a supramolecular AIE glyconanoparticle, Small 12 (2016) 6562–6567, https://doi.org/10.1002/smll.201601470.
[43] H. Blom, J. Widengren, Stimulated emission depletion microscopy, Chem. Rev. 117 (2017) 7377–7427, https://doi.org/10.1021/acs.chemrev.6b00653.
[44] J. Torra, P. Bondia, S. Gutierrez-Erlandsson, B. Sot, C. Flors, Long-term STED imaging of amyloid fibers with exchangeable Thioflavin T, Nanoscale 12 (2020) 15050–15053, https://doi.org/10.1039/D0NR02961K.
[45] Y. Yu, D.C. Jans, B. Winblad, L.O. Tjernberg, S. Schedin-Weiss, Neuronal Aβ42 is enriched in small vesicles at the presynaptic side of synapses, Life Sci. Alliance 1 (2018), e201800028, https://doi.org/10.26508/lsa.201800028.

Álvaro Ruiz-Arias is a PhD student at the 'Photochemistry and Photobiology' research group. His research focuses on the study of amyloid fibrillization using advanced microcopy techniques.

Rocío Jurado finished her PhD in the research group BioNanoMet at the University of Granada where she is currently a postdoctoral researcher at the Department of Inorganic Chemistry. Her research focuses on the investigation of hybrid nanomaterials with biomedical applications.

Francisco Fueyo-González is currently a postdoctoral researcher at the Department of Medicine, Translational Transplant Research Center, Immunology Institute, Icahn School of Medicine at Mount Sinai, New York, New York. His research interests are focused on the design, development and application of new luminescent sensors in immunology of organs transplantation.

Rosario Herranz is currently senior scientific researcher at the Medicinal Chemistry Institute of the Consejo Superior de Investigaciones Científicas (CSIC) of Spain. Her research interests have been focused on the design, synthesis and characterization of potential drug candidates towards diverse targets, particularly in the field of peptides and peptidomimetics. More recently, her interest is focus on fluorescent probes for biosensors and imaging agents.

Prof. Natividad Galvez is full Professor in Inorganic Chemistry at the University of Granada. She is co-leader of the BioNanoMet research group. Her research has focused on the synthesis and structure of new entities of nanometric size. Her group has prepared multifunctional nanostructures mainly looking for applications in Nanomedicine. Currently, her main interests lie in studying amyloid-like protein fibers as a new scaffold for the preparation of bioinorganic hybrid materials, with applications in Biomedicine.

Juan A. González-Vera is currently a lecturer in the Physical Chemistry Department at the Faculty of Pharmacy of the University of Granada (Spain). His main research interests are directed to the development of luminescent tools for the study of complex biological systems at the interface of chemistry and biology.

Prof. Angel Orte is currently full Professor in Physical Chemistry at the Faculty of Pharmacy of the University of Granada (Spain), and head of the 'FQM247-Photochemistry and Photobiology' research group. His main research interests are devoted to development of advanced fluorescence microscopy and single-molecule fluorescence tools for the study of biomedical problems, such as protein aggregation and pathological cellular processes.